778 J. Med. Chem. 2010, 53, 778–786
DOI: 10.1021/jm901440f

Journal of Medicinal Chemistry Article

Antiviral Potential and Molecular Insight into Neuraminidase Inhibiting Diarylheptanoids from *Alpinia katsumadai*

Ulrike Grienke,[†] Michaela Schmidtke,[‡] Johannes Kirchmair,[§] Kathrin Pfarr,[‡] Peter Wutzler,[‡] Ralf Dürrwald,[⊥] Gerhard Wolber,[§] Klaus R. Liedl,[∥] Hermann Stuppner,[†] and Judith M. Rollinger*[,†]

[†]*Institute of Pharmacy/Pharmacognosy and Center for Molecular Biosciences Innsbruck, University of Innsbruck, Innrain 52c, 6020 Innsbruck, Austria,* [‡]*Institute of Virology and Antiviral Therapy, Friedrich Schiller University, Hans-Knöll-Strasse 2, 07745 Jena, Germany,* [§]*Institute of Pharmacy/Pharmaceutical Chemistry and Center for Molecular Biosciences Innsbruck, University of Innsbruck, Innrain 52c, 6020 Innsbruck, Austria,* [∥]*Institute of Theoretical Chemistry and Center for Molecular Biosciences, University of Innsbruck, Innrain 52a, 6020 Innsbruck, Austria, and* [⊥]*IDT Biologika GmbH, Abteilung Forschung und Entwicklung, Am Pharmapark 1, 06861 Dessau-Rosslau, Germany*

Received September 29, 2009

At present, neuraminidase (NA) inhibitors are the mainstay of pharmacological strategies to fight against global pandemic influenza. In the search for new antiviral drug leads from nature, the seed extract of *Alpinia katsumadai* has been phytochemically investigated. Among the six isolated constituents, four diarylheptanoids showed in vitro NA inhibitory activities in low micromolar ranges against human influenza virus A/PR/8/34 of subtype H1N1. The most promising constituent, katsumadain A (**4**; $IC_{50} = 1.05 \pm 0.42\ \mu M$), also inhibited the NA of four H1N1 swine influenza viruses, with IC_{50} values between 0.9 and 1.64 μM, and showed antiviral effects in plaque reduction assays. Considering the flexible loop regions of NA, extensive molecular dynamics (MD) simulations were performed to study the putative binding mechanism of the T-shaped diarylheptanoid **4**. Docking results showed well-established interactions between the protein and the core of this novel NA-inhibiting natural scaffold, excellent surface complementarity to the simulated binding pocket, and concordance with experimentally derived SAR data.

Introduction

Influenza viruses belonging to the genera A and B are responsible for seasonal flu epidemics each year, which cause acute contagious respiratory infections. Children, the old, and people with chronic diseases are at high risk to develop severe complications that lead to high morbidity and mortality rates.[1] Among the three influenza genera, type A viruses are the most virulent human pathogens that cause the most severe disease, can be transmitted to other species, and give rise to human influenza pandemics. The recent human influenza outbreak of the aggressive porcine A/H1N1 strain in 2009 has emphasized the need for novel antiviral therapeutics. The enzyme neuraminidase (NA;[a] also known as sialidase), which is an exoglycohydrolase consisting of four identical subunits, plays a key role not only in the release of virions from infected host cells but also in their movement through the upper respiratory tract.[2] The replication of virus particles is blocked by the application of NA inhibitors, which have the ability to fit into the active site of the enzyme and avoid the cleavage of the connection between host cell and newly built virions.[3,4]

At the moment, there are four well-established anti-influenza drugs commercially available. Matrix protein 2 inhibitors, also called ion channel blockers, amantadine and rimantadine owning an adamantine scaffold are only targeting influenza type A and have the disadvantage of side effects associated with the central nervous system and the gastrointestinal tract.[2] Furthermore, the application of ion channel blockers is limited due to the rapid emergence of antiviral resistance during therapy.[5−7] Starting from Hong Kong, adamantine resistant H3N2 spread all over the world since 2003.[8−10] Resistant H1N1 emerged some years later.[11,12] Most importantly, the novel reassorted pandemic H1N1 variant from swine contains the M gene of European swine influenza A viruses known to be ion channel blocker resistant since 1989.[13,14] Therefore, infections with the pandemic H1N1 cannot be treated with this pharmacological class of anti-influenza drugs. Oseltamivir and zanamivir (Chart 1), both NA inhibitors, are the only antiviral drugs recommended for flu treatment at the moment. In contrast to zanamivir, which has to be inhaled, an advantage of oseltamivir is its easy, oral application. Both drug substances have been approved for the treatment of influenza A and B virus infections. Compared to matrix 2 ion channel blockers, they are better tolerated and have rarely shown antiviral resistance until the season 2007/2008.[3,15,16] In this season, the situation suddenly changed for the worse. Oseltamivir resistant H1N1 viruses spontaneously arose and spread globally.[17−19]

Currently circulating resistant H1N1 viruses carry the histidine-to-tyrosine (His274Tyr) substitution in NAs that confers resistance to oseltamivir but does not affect susceptibility to zanamivir. In contrast to group 1 NAs (N1, N4, N5, N8), group 2 NAs (N2, N3, N6, N7, N9) can still accommodate

*To whom the correspondence should be addressed. Phone: +43 512 507 5308. Fax: +43 512 507 2939 E-mail: judith.rollinger@uibk.ac.at.

[a] Abbreviations: CC_{50}, 50% cytotoxic concentration; EMEM, Eagle minimum essential medium; MDCK, Madin Darby canine kidney; MD, molecular dynamics; NA, neuraminidase; PDB, protein data bank; rmsd, root-mean-square deviation.

 Published on Web 12/16/2009

Chart 1. NA Inhibitors Zanamivir (A) and Oseltamivir (B)

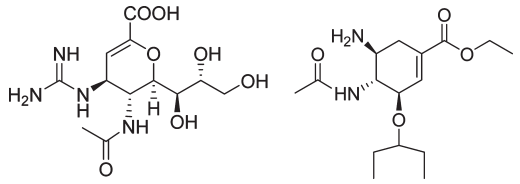

A B

oseltamivir in the binding pocket in the presence of Tyr274.[20] Oseltamivir remains a treatment option for infections with the new pandemic swine-origin H1N1 virus,[21] however, due to resistance issues, it is not appropriate for patients infected with currently circulating human H1N1.[19] Despite the recent changes in NA inhibitor susceptibility among human N1 viruses, the importance of influenza NA in viral life circle and the close correspondence of the conserved residues of the active sites of NAs from all influenza A and B viruses,[22] render the enzyme a promising target for the discovery of new drug leads to combat the pathogenesis of influenza virus infection. Additionally, the availability of, to date, around 160 NA X-ray complexes in the Protein Data Bank (PDB)[23] contributes to the attractiveness of this drug target for structure-based approaches. Thanks to these crystal structures several potent NA inhibitors, like oseltamivir and zanamivir, could be discovered.[2]

Given such issues, literature regarding NA inhibitory activity with special focus on the plant kingdom was explored. In 2003, Lee et al. investigated 260 methanolic (MeOH) extracts of oriental plant materials on NA inhibition using the in vitro method of Myers et al.[24] with some modifications.[25] The MeOH-crude extract of *Alpinia katsumadai* Hayata showed 92% inhibition at 1 ppm.[25] In addition, *A. katsumadai* is described in patents as an antiviral herbal remedy[26] and as ingredient of complex Chinese antiviral preparations.[27,28]

This information prompted us to phytochemically investigate *A. katsumadai* and to elucidate the molecular constituents responsible for the NA-inhibiting activity. As there was no information about the used organ in the publication of Lee et al., we decided to work with the seeds, which are commonly used as an herbal remedy in Traditional Chinese Medicine and recommended against "epigastric and abdominal cold pain" and for the treatment of "phlegm-dampness constraining the lungs and affecting breathing, causing fullness and a stifling sensation in the chest".[29]

In this study, we started from the most active NA-inhibiting fraction of the seeds of *A. katsumadai* and isolated six constituents, five diarylheptanoids and *trans*,*trans*-farnesol. All the diarylheptanoids showed significant NA inhibiting in vitro activities in the low micromolar range. Because the active constituents represent a novel class of NA inhibitors and differ in chemical space and shape from the lead structures oseltamivir and zanamivir (Chart 1), computational docking studies were used to rationalize the interaction in the NA binding site.

Results and Discussion

Phytochemistry. The ethanol (EtOH) extract of *A. katsumadai* semen was subjected to liquid/liquid partition using petroleum ether (PE), dichloromethane (DCM), ethyl acetate (EA), *n*-butanol (BU), and water. Because of its most promising results regarding NA inhibition (IC_{50} = 0.7 ± 0.1 μg/mL), the DCM fraction (AK_DCM) was chosen for

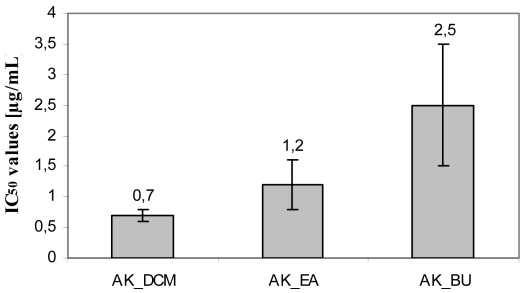

Figure 1. Inhibition of NA of influenza virus A/PR/8/34 by *A. katsumadai* extracts of different polarity as determined in chemiluminescence-based enzyme inhibition assays (n = 3, each concentration in triplicate).

phytochemical investigations (Figure 1). After several chromatographic separation steps (silica gel and Sephadex column chromatography), five diarylheptanoids and one sesquiterpene were isolated. They could be identified as (*E*,*E*)-5-hydroxy-1,7-diphenyl-4,6-heptadien-3-one (**1**), (*E*,*E*)-1,7-diphenyl-4,6-heptadien-3-one (**2**), (3*S*,5*S*)-*trans*-3,5-dihydroxy-1,7-diphenyl-1-heptene (**3**), katsumadain A (**4**), (*S*)-1,7-diphenyl-6(*E*)-hepten-3-ol (**5**), and *trans*,*trans*-farnesol (**6**) (Chart 2) by using HPLC, MS analysis, optical rotation, and 1D/2D NMR experiments and comparison with published data.

All six isolated compounds have been reported previously from the seeds of *A. katsumadai*.[30,31] However, **5** was described to be a racemate by Kuroyanagi et al.[30] Our isolate showed a negative optical rotation ($[\alpha]_D^{20}$ −6.41; c = 0.92; MeOH), which goes along with the data reported by Suksamrarn et al. for the *S*-configured enantiomer isolated from the rhizomes of *Curcuma comosa*.[32]

NA Activity. To compare the NA inhibitory activity of plant extract and selected compounds from *A. katsumadai*, influenza virus A/PR/8/34 susceptible to NA inhibition was used as test virus in chemiluminescence-based enzyme inhibition assays.[16] This assay was recommended for NA inhibitor susceptibility testing of human influenza viruses by Sheu et al.[33] and ensures a strong agreement of data received in different laboratories.[16] Using this assay, an IC_{50} of 0.13 nM was determined for oseltamivir included as positive control in the present studies. The pharmacological evaluation of three *A. katsumadai* fractions (AK_DCM, AK_EA, and AK_BU) regarding their NA inhibiting potential revealed the lowest IC_{50} value (0.7 ± 0.1 μg/mL) for the DCM fraction (Figure 1).

Four of the five diarylheptanoids, i.e., compound **1**, **2**, **4**, and **5**, isolated from the active DCM-fraction, were able to inhibit the NA in the enzyme test with IC_{50} values between 1.0 and 6.1 μM. Compound **3** and the isolated sesquiterpene **6** exerted only weak in vitro inhibitory activities (IC_{50} 29.8 μM and 81.4 μM, respectively) (Table 1). Comparison of the diarylheptanoids to *trans*,*trans*-farnesol (**6**), a C_{15}-compound without any aromatic moiety (Chart 2), reveals that the two peripheral phenyl groups with a spacer represented by the heptyl chain seem to contribute to the NA inhibitory activity. In addition, an increasing number of hydroxyl-groups in the heptyl chain connecting the two phenyl groups obviously decreases the NA inhibiting effect. This tendency was observed for **3** possessing two hydroxyl groups in contrast to **1**, **2**, **4**, and **5**. The most potent compound **4** differs from other diarylheptanoids in a monocyclic α-pyrone moiety and an additional phenyl group.

Chart 2. Chemical Structures of Diarylheptanoids (*E*,*E*)-5-Hydroxy-1,7-diphenyl-4,6-heptadien-3-one (**1**), (*E*,*E*)-1,7-Diphenyl-4,6-heptadien-3-one (**2**), (3*S*,5*S*)-*trans*-3,5-Dihydroxy-1,7-diphenyl-1-heptene (**3**), Katsumadain A (**4**), (*S*)-1,7-Diphenyl-6(*E*)-hepten-3-ol (**5**), and the Sesquiterpene *trans*,*trans*-Farnesol (**6**)

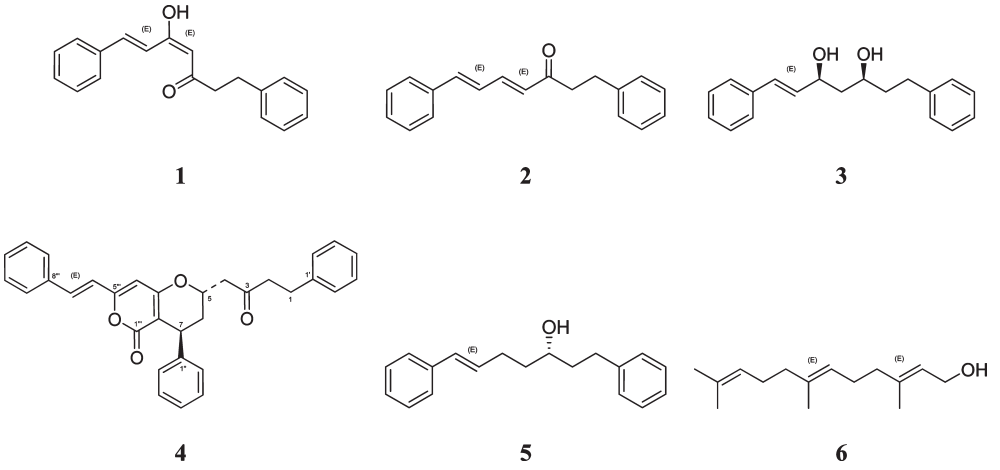

Table 1. In Vitro Inhibition of NA of Influenza Virus A/PR/8/34 by Substances Isolated from *A. katsumadai* Semen as Determined in Chemiluminescence-Based Enzyme Inhibition Assay (n = 3, Each Concentration in Triplicate)

compd	IC_{50} values [μM]
1	4.67 ± 0.36
2	6.10 ± 1.52
3	29.75 ± 8.15
4	1.05 ± 0.42
5	4.13 ± 1.50
6	81.40 ± 36.43

Table 2. NA Inhibitory Activity of Oseltamivir and **4** against Several Porcine H1N1 Isolates as well as an Oseltamivir-Resistant Human H1N1 Isolate ($n \geq 4$, Each Oseltamivir Concentration in Duplicate and Each Katsumadain A Concentration Triplicate)

	IC_{50} of	
influenza virus	oseltamivir (nM)	katsumadain A (**4**) (μM)
A/Potsdam/15/81[a]	0.16	0.73
A/Belzig/2/01[a]	0.20	0.59
A/Horneburg/IDT7489/08	0.06	1.11
A/Brest/IDT7490/08	0.19	1.64
A/342/09[b]	resistant[c]	maximum inhibition 45.9%[d]

[a] One assay with each oseltamivir concentration in duplicate; each concentration of compound **4** in triplicate. [b] Oseltamivir-resistant human H1N1 isolate. [c] Maximum tested concentration: 100 nM. [d] Used test concentration 52.5 μM.

In addition to the M gene, the novel pandemic H1N1 virus received also the NA gene from European swine viruses. Therefore, we decided to test the inhibitory potential of the most active diarylheptanoid, i.e., compound **4**, against NA of four swine viruses isolated from ill pigs in Germany between 1981 and 2008. Oseltamivir was included as control in these studies. The results are summarized in Table 2. Oseltamivir inhibited the NA of all tested H1N1 swine viruses at nanomolar concentrations between 0.06 and 0.20 nM. The determined IC_{50} values strongly correspond with that published for swine H3N2 as well as human influenza A viruses.[16,33,34]

The IC_{50} values determined for **4** varied between 0.59 and 1.64 μM (Table 2). They indicate a good NA inhibitory activity of **4** against swine influenza A isolates of subtype H1N1. The NA of the oseltamivir-resistant human H1N1 isolate A/342/09 exhibited a markedly lower susceptibility to this compound. The addition of 6.6 to 52.5 μM of **4** led to a NA inhibition ranging from 27.0% to maximally 45.9%, respectively.

Cytotoxicity and Antiviral Activity of Katsumadain A (4) in MDCK Cells. Compound **4** was well tolerated in confluent MDCK cell monolayers with a 50% cytotoxic concentration (CC_{50}) of 66.9 μM. Its antiviral activity was determined in plaque reduction assays with influenza A/PR/8/34 in MDCK cells. This human H1N1 virus is oseltamivir-susceptible in cell culture-based assays with a mean IC_{50} of 194.1 nM. The studies with **4** revealed an IC_{50} value of 11.75 ± 3.42 μM and underline the anti-influenza virus activity of the tested compound.

Computational Docking. X-ray crystallographic studies on influenza NA indicate significant flexibility of the 150-loop.[35] On the basis of these experimental observations, Amaro et al. performed in-depth analyses of the conformational behavior of influenza NA using molecular dynamics (MD) simulation techniques,[36,37] with focus on the 150-loop. These computational studies confirmed a high degree of conformational flexibility in this region but also in the neighboring 430-loop. These conformational shifts could be exploited to accommodate novel, bulkier, and more potent binders. In a following study, Cheng et al. proposed novel compounds based on docking studies using a representative open-conformation frame of this MD simulation.[38]

In this study, among all tested compounds, **4** showed the highest inhibitory activity of influenza NA. At the same time, this compound considerably differs from known active NA inhibitors in terms of shape and size, which makes the exploration of the binding mode of this novel class of inhibitors interesting for detailed modeling studies. Moreover, the rigidity of this compound makes it the best choice for docking studies in order to derive a binding hypothesis. Recently, An et al. have analyzed the putative binding mode of a novel NA inhibitor, 4-(4-((3-(2-amino-4-hydroxy-6-methyl-5-pyrimidinyl)propyl)amino)phenyl)-1-chloro-3-buten-2-on, using ICM-based[39] protein−ligand docking.[40] As we found GOLD[41] in combination with GOLDScore to

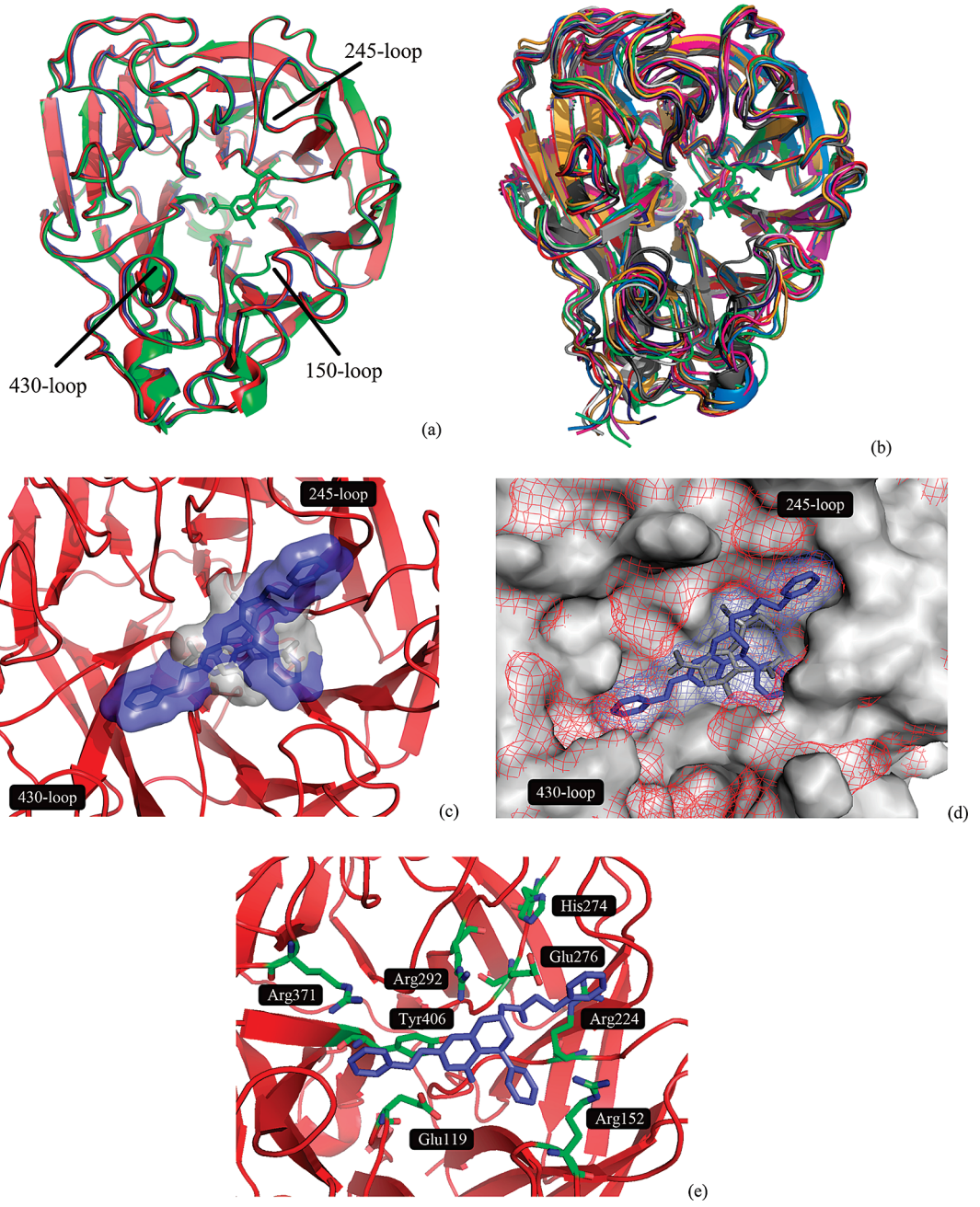

Figure 2. Elucidation of the putative binding mode of compound **4**. (a) Overlay of the X-ray structures used for docking. The closed conformation (2hu4) is indicated in green color with oseltamivir bound. The open apo-structure (2hty) is indicated in red color, and the open holo-structure (2hu0) is indicated in blue color, respectively. Oseltamivir forms a strong H-bonding network and charged interactions with the neighboring Arg118, Arg152, Arg292, and Arg371. Moreover, the branched alkyl moiety establishes tight surface contacts with Arg224 and Glu276. (b) Overlay of the 10 representative MD frames used for docking. The residues involved in the binding of oseltamivir mainly show moderate conformational flexibility. Hereby, a certain degree of flexibility is observed in particular for residues Arg156 and Arg371. Significant conformational shifts are evident for residues forming the 150- and 430-loop; some degree of conformational flexibility is also observable for the 245-loop. The X-ray structures are indicated in gray color, and the representative frame four is indicated in red color, respectively. This MD frame is embedded well among the 10 representative MD frames. It is related to the X-ray open conformation but shows an extended binding pocket nearby the 430- and the 150-loop. (c) Oseltamivir bound to NA, in comparison to **4**. The core of **4** (violet color) exactly matches the location of the bound oseltamivir (gray color). (d) Surface complementarity of compound **4** and the representative frame four. Compound **4** (blue color, blue mesh) shows optimum surface complementarity with the target structure, indicating a strong entropic contribution to the protein−ligand binding free energy. The illustration highlights the conformational differences between the X-ray open conformation (2hty, red mesh) and the MD frame (gray surface). In particular, the more opened conformation of the 430- and the 245-loops is essential for accommodating the ligand. (e) Compound **4** docked to NA representative frame for cluster 4 (red color), with interacting residues indicated in green color. The ensemble of protein−ligand interactions observed for **4** is characterized by hydrophobic interactions of the peripheral aromatic substituents (as well as the alkene chain) and the simultaneous formation of cation−π interactions with Arg152, Arg224, and Arg371. H-bonds are formed between the cyclic ether and Arg292 and between the lactone and Glu119. Furthermore, considering the hydrophilic parts of the binding pocket and the geometry of the ligand pose, water-mediated hydrogen bonds are likely to establish interactions between the protein and the ligand lactone group. In the case of a His274Tyr mutation, a shift of Glu276 toward the binding pocket is likely to cause repulsion of the ligand from the binding pocket.

perform particularly well in prior redocking studies, we chose this software to analyze the binding mode of **4** (more information on the computational approach is provided in the Experimental Section). Initial experiments using an X-ray model of the closed conformation of NA (PDB entry 2hu4, Figure 2a) strongly indicated that the large, T-shaped compound **4** is unlikely to bind to the target in its closed conformation; the binding area is too small to accommodate the ligand. Using open-conformation NA structures (PDB codes 2hty and 2hu0, Figure 2a) allowed us to obtain a few docking poses that came fairly close to a reasonable binding hypothesis, fulfilling requirements for protein−ligand interactions and surface complementarity. However, the poses of 10 individual docking runs for each X-ray structure were scattered all over the binding pocket. Being aware of the considerable flexibility of parts of the NA, this strongly indicates possible structural shortcomings in the experimental determination of the target conformation, making it unfeasible to determine the putative binding mode. Moreover, moieties of even the most plausible docking poses seemed not to be placed favorably in the binding pocket, which is a common observation when using a rigid receptor docking approach.

To enhance docking predictions, we performed a MD simulation of the apo protein system (PDB entry 2hty) using AMBER 10[42] to account for protein flexibility (more information on the computational approach is provided in the Experimental Section). Ten representative frames of the 20 ns trajectory were selected for analyses (Figure 2b), and 10 individual docking runs were processed for each of these frames. The conformations we observed during the MD simulation compare very well to the conformational flexibility reported in recent studies mentioned above.[36,37] They share a comparable, limited degree of flexibility of the protein moieties involved in the formation of the oseltamivir binding pocket and a considerable degree of conformational flexibility in 150- and 430-loops. The behavior of both flexible loops is in concordance with the conformations reported by MD studies of Amaro et al.[36,37]

Analysis of the docking poses was started by generating a rank-ordered list of all docking poses of all frames based on their GOLDScore. We found that the highest-ranked pose is obtained for the representative frame of cluster 4 (GOLDScore 74.14), which is the second most-populated cluster of protein conformations observed during MD simulations (Figure 3a,b). However, ranking compounds exclusively by scoring functions is considered problematic.[43] Therefore, we looked at the overall arrangement of the docking poses within the binding site. For the majority of the frames, the poses were scattered more or less among the binding site and no obvious preferences for a binding mode could be revealed. For cluster 4, however, we found a surprising agreement for ligand placement: all 10 poses of cluster 4 are consistent, almost identical. Together with the highest GOLDScore, this is another strong indicator for the reliability of the predicted binding mode. Intriguingly, the ligand core matches the binding location of the two closely related and comparably binding NA inhibitors oseltamivir (Figure 2c) and zanamivir (not shown). Even more interesting, the ligand placement shows optimum surface complementarity with the binding pocket (Figure 2d), suggesting a strong entropic benefit upon ligand binding. The docked ligand also shows a well-formed hydrogen bonding network with the protein environment, which is discussed in more detail in Figure 2e. For the other

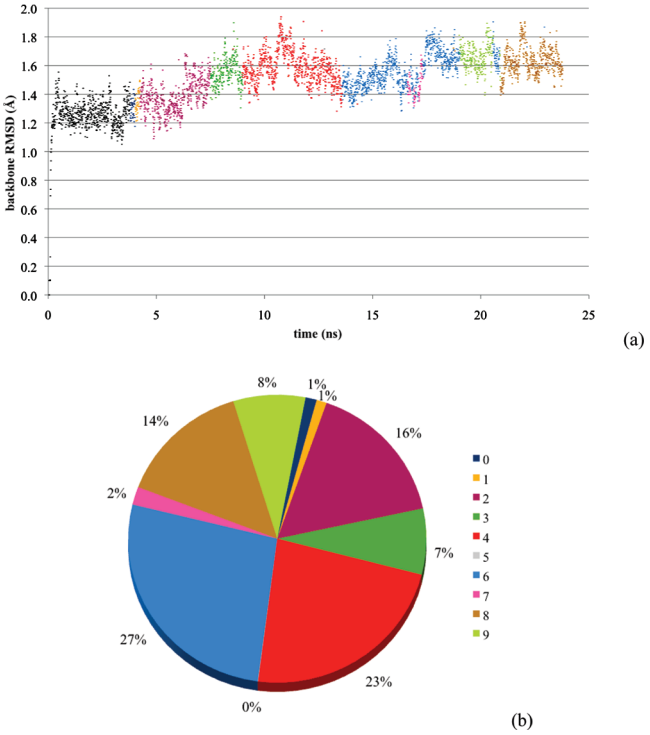

Figure 3. For the selection of representative frames observed during the molecular dynamics studies, the trajectory was clustered into 10 clusters employing the average linkage algorithm as implemented in AMBER 10. (a) rmsd plot of the protein backbone (colors as reported in Figure 3b, in accordance with the color coding of the protein conformations presented in Figure 2b; the equilibration and initial MD simulation phase which have not been considered for trajectory clustering are indicated in black color). Each data point represents a trajectory frame used for clustering. The figure demonstrates the stability of cluster 4 over several nanoseconds. A representative frame of this cluster led us to the putative binding mode of compound **4**. (b) Cluster population of the 10 clusters. Cluster 4 accounts for one-quarter of the snapshots extracted during MD simulations.

nine MD frames, we found no docking poses that show a comparable degree of plausibility except some individually placed poses that are in agreement with the poses of frame four. Intriguingly, compound **4** shows considerably lower activity against the oseltamivir-resistant human H1NI isolate. It is known (according to the German Reference Laboratory for influenza viruses at the Robert-Koch-Institute Berlin that provided us with the oseltamivir-resistant virus as control for antiviral testing) that this virus carries the His274Tyr mutation that imparts oseltamivir resistance. Looking at the proposed binding mode of compound **4** to NA (Figure 2e), it is obvious that a conformational shift of Glu276 induced by this mutation[20] causes a reduction of the binding site in this key interaction area and, hence, the repulsion of the ligand. In a docking simulation using the mutated protein structure, we were unable to dock the ligand in a comparable docking pose into the binding pocket. Overall, several indicators render the proposed binding mode of compound **4** highly likely. First, the ligand pose obtains the highest docking score for compound **4** among all protein frames and docking poses and statistical analyses on the MD trajectory prove the high population of this cluster of protein conformations. Second, the geometric agreement of all binding poses for this representative trajectory frame is another sign for the plausibility of the proposed binding

mode. In this pose, the ligand exhibits a well-established network of interactions and excellent surface complementarity with the target protein. Strikingly, also, the experimentally observed activity variations of wild type and mutant NA agree with the proposed binding mode of compound **4**.

Conclusions

The appearance of drug-resistant influenza-viruses and the threat of pandemics demonstrate a high need in the search for innovative and effective antiviral agents.[44] In this study, we focused on the phytochemical investigation and pharmacological evaluation of the medicinal plant *A. katsumadai* combined with a theoretical computational docking approach considering the flexibility of the target enzyme NA.

Our results show that four out of six isolated compounds possess NA inhibiting IC_{50} values against human influenza A virus of subtype H1N1 in low micromolar ranges. Interestingly, the structure of compound **4**, the most active NA inhibitor, is approximately 50% larger than the well established drugs oseltamivir and zanamivir. Despite this fact a promising NA-inhibiting potential could be attested to this diarylheptanoid not only against human but also against four swine influenza A viruses of subtype H1N1. However, compound **4** exhibited only a weak effect against the oseltamivir-resistant human H1N1 isolate A/342/09.

We showed that the isolation of compounds from natural sources in combination with computational techniques, namely MD simulations, might play an important role for the discovery of novel antiviral-drug leads. On the basis of the NA X-ray crystal structures alone, the elucidation of a plausible binding mode for this novel class of NA inhibitor was not possible, because flexible loop regions are not apparent in these structures. Therefore, MD studies revealed as essential to render the conformational space of the target an extended binding pocket conformation. The applied in silico technique allowed accommodating compound **4** and rationalizing its putative interaction in the NA binding site. This molecular insight will help to increase the knowledge in ligand-target interactions of this flexible NA binding pocket and to derive more potent ligands based on this novel natural scaffold.

Experimental Section

General Experimental Procedures. Optical rotations were measured on a Perkin-Elmer 341 polarimeter at 25 °C. The NMR experiments were accomplished on a Bruker DRX300 at 300 K in $CDCl_3$ (calibrated to the residual nondeuterated solvent signals). MS analysis was performed on an Esquire 3000 plus ion-trap mass spectrometer (Bruker Daltonics) equipped with electrospray ionization (ESI) in positive and negative mode: spray voltage, 4.5 kV; sheath gas, N_2, 30 psi; dry gas, N_2, 6 L min^{-1}, 350 °C; scanning range, m/z 50−1000. Column chromatography was performed using Merck silica gel 60, 40−63 μm and Pharmacia Sephadex LH-20, 20−100 μm. The obtained fractions from all chromatographic steps were analyzed by TLC (mobile phase: DCM:EA [9:1]; stationary phase: Merck silica gel 60 PF_{254}, detected with staining reagents vanillin/H_2SO_4 at VIS, UV 254, UV 366). HPLC was performed on a Hewlett-Packard HP-1100 system with a photodiode array detector (DAD). LC-parameters: stationary phase: Zorbax SB-C_{18}, Rapid Resolution 3.5 μm (4.6 mm × 150 mm), Agilent, USA; temperature: 40 °C; mobile phase: water (A); acetonitrile (B); flow rate 1.0 mL/min; UV detection wavelength: 205, 280, 360 nm; injection volume: 10 μL; gradient: 70% A, 30% B; 35 min; 55% A, 45% B; 40 min; 35% A, 65% B; 62 min; 2% A, 98% B. All chemicals and solvents used were analytical grade.

Plant Material. The dried seeds of *Alpinia katsumadai* Hayata, Zingiberaceae were obtained from Plantasia (MMag. Erich A. Stöger, Oberndorf/Salzburg, Austria). The quality was checked according to the monograph cão dòu kòu of the Chinese Pharmacopoeia. A voucher specimen (JR-20070315-A1) is deposited in the Herbarium of the Institute of Pharmacy/Pharmacognosy, LFU, Innsbruck, Austria.

Extraction and Isolation. First, 1384 g crushed seeds of *A. katsumadai* were macerated with EtOH (4.5 L at RT, three times for 4 days each). After removal of the solvent under vacuum, the EtOH extract yielded 68.8 g. This EtOH extract was partitioned between PE, DCM, EA, BU, and water. Thereby obtained solvent fractions were evaporated under vacuum. The DCM fraction (21.35 g) was subjected to silica column chromatography (Merck silica gel 60 PF_{254}, 213 g; 65 cm × 4 cm) using a gradient system of *n*-hexane-DCM-EA (300:0:0, 80:20:0, 330:330:0, 60:240:0, 0:1500:0, 0:480:120, 0:105:45 mL) to give 15 fractions (A1−15). Fraction A4 (75.77 mg) was further separated using Sephadex LH 20 column chromatography (mobile phase: DCM/acetone (85:15)) to yield four fractions (B1−4). 15.71 mg of compound **1** were obtained by recrystallization of fraction B2 (orange−yellow needles) from MeOH. Fraction A6 (2057.71 mg) was purified via Sephadex LH 20 column chromatography (mobile phase: DCM/acetone (85:15)) to give two fractions (C1−2). Then 1328.28 mg of compound **2** were gained from C2 (yellow needles). Fraction A7 (605.35 mg) was chromatographed by Sephadex LH 20 (mobile phase: DCM/acetone (85:15)) to give seven fractions (D1−7). D3 (110.68 mg) was identical to compound **2**. Fraction A8 (899.95 mg) was subjected to Sephadex LH 20 column chromatography (mobile phase: MeOH) yielding three fractions (E1−3). Fraction E3 could be obtained as pure compound **4** (light-yellow amorphous solid) (127.80 mg), whereas fractions E1 and E2 were rechromatographed for purification on Sephadex LH 20 column chromatography (mobile phase: MeOH) to give 3 fractions each (F1−3 and G1−3). **6** (F1) (123.58 mg of pale-yellow liquid) and 35.9 mg of **5** (G3) (colorless liquid) were obtained. Fraction A13 (1581.46 mg) was separated by Sephadex LH 20 column chromatography (mobile phase: MeOH) to obtain three fractions (H1−3). Then 1060.05 mg of compound **3** (colorless needle) were gained from H1. The physical and spectroscopic data of compounds **1**−**6** agree with those previously published[30−32] for (*E*,*E*)-5-hydroxy-1,7-diphenyl-4,6-heptadien-3-one (**1**), (*E*,*E*)-1,7-diphenyl-4,6-heptadien-3-one (**2**), (3*S*,5*S*)-*trans*-3,5-dihydroxy-1,7-diphenyl-1-heptene (**3**), katsumadain A (**4**), (*S*)-1,7-diphenyl-6(*E*)-hepten-3-ol (**5**), and *trans*, *trans*-farnesol (**6**). Their purity was determined by HPLC to be ≥98%.

Katsumadain A (4). Light-yellow amorphous solid; $[\alpha]_D^{20}$ +1.19 (c = 1.09; EtOH). ^{1}H NMR (300 MHz, $CDCl_3$) δ: 2.91 (2H, m, H-1), 2.78 (2H, m, H-2), 2.85 (1H, dd, H-4), 2.51 (1H, dd, H-4), 4.49 (1H, m, H-5), 2.02 (2H, m, H-6), 4.13 (1H, t, H-7), 5.93 (1H, s, H-4‴), 6.58 (1H, d, H-6‴), 7.49 (1H, d, H-7‴), 7.37−7.18 (15H, overlapping, aromatic protons). ^{13}C NMR (300 MHz, $CDCl_3$) δ: 29.8 (C-1), 45.5 (C-2), 206.5 (C-3), 48.0 (C-4), 69.9 (C-5), 35.4 (C-6), 35.4 (C-7), 141.1 (C-1′), 143.5 (C-1″), 163.3 (C-1‴), 101.4 (C-2‴), 165.5 (C-3‴), 101.1 (C-4‴), 158.1 (C-5‴), 119.1 (C-6‴), 135.6 (C-7‴), 135.7 (C-8‴), 129.2−126.7 (aromatic carbons). The data is in agreement with the data reported by Yang et al.[31]

Cells and Viruses. MDCK cells (Friedrich-Loeffler Institute, Riems, Germany) were grown in Eagle minimum essential medium (EMEM) supplemented with 10% fetal bovine serum, 100 U/mL penicillin, and 100 U/mL streptomycin. Medium applied in plaque reduction assays was formulated with 2 μg/mL trypsin and 1.2 mM bicarbonate and did not contain serum.

A/Horneburg/IDT7489/08 and Brest/IDT490/08 were isolated in embryonated hens eggs from nasal swabs obtained from pigs with clinical symptoms.

Stocks of H1N1 influenza virus A/PR/8/34 (Institute of Virology, Philipps University, Marburg), the oseltamivir-resistant human H1N1 isolate A/342/09 (Robert Koch Institute, Berlin, Germany) and the porcine H1N1 isolates A/Belzig/2/01, A/Potsdam/15/81 (Dr. Schrader, Bundesinstitut für Risikoforschung, Berlin, Germany), A/Horneburg/IDT7489/08, and Brest/IDT490/08 were propagated in MDCK cells, aliquoted, and stored at −80 °C until use.

Compound Preparations. Oseltamivir carboxylate (GS4071) was kindly provided by F. Hoffmann-La Roche AG (Basel, Switzerland; lot no. RO0640802-002). Compound stock was prepared in water and stored at 4 °C. Stock solutions of compounds **1**−**6** were prepared in DMSO.

Chemiluminescence-Based NA Inhibition Assay. NA inhibition was determined with the commercially available NA-Star kit (Tropix, Applied Biosystems, Darmstadt, Germany) that utilizes a 1,2-dioxetane sialic acid derivative for the substrate, according to the protocol of the manufacturer and as described recently.[16,40] At first, each individual virus culture supernatant was diluted in NA-Star buffer (serial 2-fold dilutions) in the absence of NA inhibitor. The virus dilution resulting in a signal-to-noise ratio of 40:1 was used then for subsequent IC_{50} determinations. Briefly, 25 μL of assay buffer (for the six virus controls included on each plate) or test compounds and oseltamivir at two times the desired concentration were added (each concentration in duplicate or triplicate, oseltamivir and test compounds **1**−**6**, respectively in assay buffer) to a 96-well microtiter plate. Afterward, 25 μL of the respective virus dilutions were added to each well, mixed with the compounds, and incubated at 37 °C for 20 min. At the end of the incubation time the substrate was diluted 1:500 in assay buffer and added to each well (10 μL) for 30 min at room temperature. The mean NA activity of the six untreated virus controls was set to 100%, and the concentration required to reduce NA enzyme activity of virus controls by 50% was calculated.

Determination of Cytotoxicity and Antiviral Activity of Katsumadain A (4) in MDCK Cells. Cytotoxicity as well as antiviral activity of test compounds was determined on 3-day-old MDCK cell monolayers as described previously.[45] Briefly, to determine the CC_{50}, confluent cell monolayer grown in 96-well plates were incubated with serial 2-fold dilutions (each in triplicate) of **4** for 72 h (37 °C, 5% CO_2). Then the cells were fixed and stained with a crystal violet formalin solution. After dye extraction, the optical density of individual wells was quantified spectrophotometrically at 550/630 nm with a microplate reader. Cell viability of individual compound-treated wells was evaluated as the percentage of the mean value of optical density resulting from six mock-treated cell controls which was set 100%. The CC_{50} was defined as the compound concentration reducing the viability of untreated cell cultures by 50%. It was calculated from the mean dose−response curve of two independent assays.

Plaque reduction assay was used for antiviral testing with influenza virus A/Puerto Rico/8/34 on MDCK cell. Cell monolayers were inoculated with approximately 70 plaque forming units (pfu) of the virus and overlaid with 0.4% agar supplemented with serial 2-fold compound concentrations, each tested in duplicate. One uninfected, untreated cell control as well as three infected untreated virus controls were included in all assays. After 48 h of incubation at 37 °C, plates were fixed and stained with a crystal violet formalin solution, the number of virus-induced plaques was counted, and the compound-induced plaque reduction calculated. The concentration required to reduce the plaque number by 50% was calculated from the mean dose−response curves of at least 2 independent assays.

MD Simulations. AMBER 10 was used for MD simulations of chain B of PDB entry 2hty, following the approach of Amaro et al.[36,37] We prepared the system and protonated the target according to pH 6.5 using the pdb2pqr server.[46,47] Crystal waters were preserved 5 Å around the protein using VMD,[48] and the protein was solvated in a TIP3P water box placed 10 Å around the macromolecule. Rectangular periodic boundary conditions and the particle mesh Ewald approach were applied for calculating electrostatics (cutoff 10 Å). An initial minimization limited to solvent molecules was performed for 500 steepest descent minimization cycles and 500 conjugate gradient cycles. This was followed by a minimization of the full system for 2500 cycles using the steepest descent algorithm and 2500 cycles using the conjugate gradient algorithm. The system was gradually warmed to 300 K over the initial 50 ps of the simulation by applying weak restraints to the protein. An equilibration step of 100 ps under constant pressure was performed, allowing the water molecules to relax. The production MD was processed with a 2 fs time step and the SHAKE algorithm keeping all bond lengths involving hydrogens fixed. A 20 ns section of the trajectory was submitted to frame clustering.

Clustering of the Trajectory. To obtain 10 representative protein conformations for ligand docking, the trajectory was clustered considering the conformational flexibility (in terms of the backbone rmsd) of all residues of the first shell building the binding concavity of NA (residues 114−119, 134−140, 145−152, 156, 178−180, 222−227, 244−246, 276−277, 292, 294, 347−350, 371, 403−406, 423, 425−432, 437−441). AMBER 10 has included 11 different algorithms that allow for clustering trajectories. Shao et al.[49] provided an excellent in-depth analysis of the performance of these different algorithms, their advantages and disadvantages. On the basis of their observations, we selected the average linkage algorithm for clustering our trajectory (using default settings).[49]

Protein−Ligand Docking. GOLD 4.1[41] was used for docking **4** to the X-ray structures and MD frames. The 3D seed structure was generated from scratch using Corina 3.0.0.[50−52] Default settings were applied for flexible ligand docking in GOLD, except early termination was deactivated. Ten poses were calculated for each protein conformation and GOLDScore was applied for pose ranking. The protein−ligand complexes were visualized using PyMol 1.0.[53]

Acknowledgment. We thank Dr. Ernst P. Ellmerer (Institute of Organic Chemistry, University of Innsbruck) for NMR measurements and MMag. Erich Stöger (Plantasia, Oberndorf/Salzburg, Austria) for providing the plant material free of charge.

References

(1) Memoli, M. J.; Morens, D. M.; Taubenberger, J. K. Pandemic and seasonal influenza: therapeutic challenges. *Drug Discovery Today* **2008**, *13*, 590–595.
(2) von Itzstein, M. The war against influenza: discovery and development of sialidase inhibitors. *Nat. Rev. Drug Discovery* **2007**, *6*, 967–974.
(3) Moscona, A. Neuraminidase inhibitors for influenza. *N. Engl. J. Med.* **2005**, *353*, 1363–1373.
(4) Matrosovich, M. N.; Matrosovich, T. Y.; Gray, T.; Roberts, N. A.; Klenk, H.-D. Neuraminidase is important for the initiation of influenza virus infection in human airway epithelium. *J. Virol.* **2004**, *78*, 12665–12667.
(5) Hayden, F. G.; Hay, A. J. Emergence and transmission of influenza A viruses resistant to amantadine and rimantadine. *Curr. Top. Microbiol. Immunol.* **1992**, *176*, 119–130.
(6) Klimov, A. I.; Rocha, E.; Hayden, F. G.; Shult, P. A.; Roumillat, L. F.; Cox, N. J. Prolonged shedding of amantadine-resistant influenza A viruses by immunodeficient patients: Detection by polymerase chain reaction-restriction analysis. *J. Infect. Dis.* **1995**, *172*, 1352–1355.
(7) Shiraishi, K.; Mitamura, K.; Sakai-Tagawa, Y.; Goto, H.; Sugaya, N.; Kawaoka, Y. High frequency of resistant viruses harboring different mutations in amantadine-treated children with influenza. *J. Infect. Dis.* **2003**, *188*, 57–61.

(8) Simonsen, L.; Viboud, C.; Grenfell, B. T.; Dushoff, J.; Jennings, L.; Smit, M.; Macken, C.; Hata, M.; Gog, J.; Miller, M. A.; Holmes, E. C. The genesis and spread of reassortment human influenza A/H3N2 viruses conferring adamantane resistance. *Mol. Biol. Evol.* **2007**, *24*, 1811–1820.
(9) Schmidtke, M.; Bauer, K.; Ludwig, N.; Wutzler, P. Emergence and phylogenetic relationships of amantadine-resistant human H3N2 influenza A viruses in Germany in the season 2005/2006. *Int. J. Antimicrob. Agents* **2008**, *32*, 192–195.
(10) Nelson Martha, I.; Simonsen, L.; Viboud, C.; Miller Mark, A.; Holmes Edward, C. The origin and global emergence of adamantane resistant A/H3N2 influenza viruses. *Virology* **2009**, *388*, 270–278.
(11) Deyde, V. M.; Xu, X.; Bright, R. A.; Shaw, M.; Smith, C. B.; Zhang, Y.; Shu, Y.; Gubareva, L. V.; Cox, N. J.; Klimov, A. I. Surveillance of resistance to adamantanes among influenza A(H3N2) and A(H1N1) viruses isolated worldwide. *J. Infect. Dis.* **2007**, *196*, 249–257.
(12) Barr, I. G.; Hurt, A. C.; Deed, N.; Iannello, P.; Tomasov, C.; Komadina, N. The emergence of adamantane resistance in influenza A(H1) viruses in Australia and regionally in 2006. *Antivir. Res.* **2007**, *75*, 173–176.
(13) Schmidtke, M.; Zell, R.; Bauer, K.; Krumbholz, A.; Schrader, C.; Suess, J.; Wutzler, P. Amantadine resistance among porcine H1N1, H1N2, and H3N2 influenza A viruses isolated in Germany between 1981 and 2001. *Intervirology* **2006**, *49*, 286–293.
(14) Krumbholz, A.; Schmidtke, M.; Bergmann, S.; Motzke, S.; Bauer, K.; Stech, J.; Duerrwald, R.; Wutzler, P.; Zell, R. High prevalence of amantadine resistance among circulating European porcine influenza A viruses. *J. Gen. Virol.* **2009**, *90*, 900–908.
(15) Hayden, F. G. Antivirals for influenza: Historical perspectives and lessons learned. *Antivir. Res.* **2006**, *71*, 372–378.
(16) Bauer, K.; Richter, M.; Wutzler, P.; Schmidtke, M. Different neuraminidase inhibitor susceptibilities of human H1N1, H1N2, and H3N2 influenza A viruses isolated in Germany from 2001 to 2005/2006. *Antivir. Res.* **2009**, *82*, 34–41.
(17) Meijer, A.; Lackenby, A.; Hungnes, O.; Lina, B.; van-der-Werf, S.; Schweiger, B.; Opp, M.; Paget, J.; van-de-Kassteele, J.; Hay, A.; Zambon, M. Oseltamivir-resistant influenza virus A (H1N1), Europe, 2007−08 season. *Emerg. Infect. Dis.* **2009**, *15*, 552–560.
(18) Moscona, A. Global transmission of oseltamivir-resistant influenza. *N. Engl. J. Med.* **2009**, *360*, 953–956.
(19) Weinstock, D. M.; Zuccotti, G. The evolution of influenza resistance and treatment. *JAMA, J. Am. Med. Assoc.* **2009**, *301*, 1066–1069.
(20) Collins, P. J.; Haire, L. F.; Lin, Y. P.; Liu, J.; Russell, R. J.; Walker, P. A.; Skehel, J. J.; Martin, S. R.; Hay, A. J.; Gamblin, S. J. Crystal structures of oseltamivir-resistant influenza virus neuraminidase mutants. *Nature* (*London*) **2008**, *453*, 1258–1261.
(21) Itoh, Y.; Shinya, K.; Kiso, M.; Watanabe, T.; Sakoda, Y.; Hatta, M.; Muramoto, Y.; Tamura, D.; Sakai-Tagawa, Y.; Noda, T.; Sakabe, S.; Imai, M.; Hatta, Y.; Watanabe, S.; Li, C.; Yamada, S.; Fujii, K.; Murakami, S.; Imai, H.; Kakugawa, S.; Ito, M.; Takano, R.; Iwatsuki-Horimoto, K.; Shimojima, M.; Horimoto, T.; Goto, H.; Takahashi, K.; Makino, A.; Ishigaki, H.; Nakayama, M.; Okamatsu, M.; Takahashi, K.; Warshauer, D.; Shult, P. A.; Saito, R.; Suzuki, H.; Furuta, Y.; Yamashita, M.; Mitamura, K.; Nakano, K.; Nakamura, M.; Brockman-Schneider, R.; Mitamura, H.; Yamazaki, M.; Sugaya, N.; Suresh, M.; Ozawa, M.; Neumann, G.; Gern, J.; Kida, H.; Ogasawara, K.; Kawaoka, Y. In vitro and in vivo characterization of new swine-origin H1N1 influenza viruses. *Nature* (*London*) **2009**, *460*, 1021–1025.
(22) Liu, A.-L.; Wang, Y.-T.; Du, G.-H. Neuraminidase as a target for drugs for the treatment of influenza. *Drugs Future* **2005**, *30*, 799–806.
(23) Berman, H. M.; Westbrook, J.; Zardecki, C.; Bourne, P. E. The protein data bank. *Protein Struct.* **2003**, 389–405.
(24) Myers, R. W.; Lee, R. T.; Lee, Y. C.; Thomas, G. H.; Reynolds, L. W.; Uchida, Y. The synthesis of 4-methylumbelliferyl alpha-ketoside of *N*-acetylneuraminic acid and its use in a fluorometric assay for neuraminidase. *Anal. Biochem.* **1980**, *101*, 166–174.
(25) Lee, C. H.; Kim, S. I.; Lee, K. B.; Yoo, Y. C.; Ryu, S. Y.; Song, K. S. Neuraminidase inhibitors from *Reynoutria elliptica*. *Arch. Pharm. Res.* **2003**, *26*, 367–374.
(26) Wang, Z.; Huang, W.; Li, Y. Antiviral activity of extracts from *Alpinia*. Canadian Patent CN 16988472005, **2005**.
(27) Wu, J. Manufacture of traditional Chinese medicine with antiviral, anti-inflammatory, and detoxicating effects. Canadian Patent CN 18401472006, **2006**.
(28) Wang, X.; Wang, L. Topical chinese medicinal preparation with good antiviral effect. Canadian Patent CN 1012191962008, **2008**.
(29) Bensky, D.; Clavey, S.; Stöger, E.; Gamble, E. *Chinese Herbal Medicine—Materia Medica*. 3rd ed.; Eastland Press, Inc.: Seattle, 2004; pp 485−486.
(30) Kuroyanagi, M.; Noro, T.; Fukushima, S.; Aiyama, R.; Ikuta, A.; Itokawa, H.; Morita, M. Studies on the constituents of the seeds of *Alpinia katsumadai* Hayata. *Chem. Pharm. Bull.* **1983**, *31*, 1544–1550.
(31) Yang, Y.; Kinoshita, K.; Koyama, K.; Takahashi, K.; Tai, T.; Nunoura, Y.; Watanabe, K. Two novel anti-emetic principles of *Alpinia katsumadai*. *J. Nat. Prod.* **1999**, *62*, 1672–1674.
(32) Suksamrarn, A.; Ponglikitmongkol, M.; Wongkrajang, K.; Chindaduang, A.; Kittidanairak, S.; Jankam, A.; Yingyongnarongkul, B.-e.; Kittipanumat, N.; Chokchaisiri, R.; Khetkam, P.; Piyachaturawat, P. Diarylheptanoids, new phytoestrogens from the rhizomes of *Curcuma comosa*: isolation, chemical modification and estrogenic activity evaluation. *Bioorg. Med. Chem.* **2008**, *16*, 6891–6902.
(33) Sheu, T. G.; Deyde, V. M.; Okomo-Adhiambo, M.; Garten, R. J.; Xu, X.; Bright, R. A.; Butler, E. N.; Wallis, T. R.; Klimov, A. I.; Gubareva, L. V. Surveillance for neuraminidase inhibitor resistance among human Influenza A and B viruses circulating worldwide from 2004 to 2008. *Antimicrob. Agents Chemother.* **2008**, *52*, 3284–3292.
(34) Bauer, K.; Schrader, C.; Suess, J.; Wutzler, P.; Schmidtke, M. Neuraminidase inhibitor susceptibility of porcine H3N2 influenza A viruses isolated in Germany between 1982 and 1999. *Antivir. Res.* **2007**, *75*, 219–226.
(35) Russell, R. J.; Haire, L. F.; Stevens, D. J.; Collins, P. J.; Lin, Y. P.; Blackburn, G. M.; Hay, A. J.; Gamblin, S. J.; Skehel, J. J. The structure of H5N1 avian influenza neuraminidase suggests new opportunities for drug design. *Nature* **2006**, *443*, 45–49.
(36) Amaro, R. E.; Cheng, X. L.; Ivanov, I.; Xu, D.; McCammon, J. A. Characterizing Loop Dynamics and Ligand Recognition in Human- and Avian-Type Influenza Neuraminidases via Generalized Born Molecular Dynamics and End-Point Free Energy Calculations. *J. Am. Chem. Soc.* **2009**, *131*, 4702–4709.
(37) Amaro, R. E.; Minh, D. D. L.; Cheng, L. S.; Lindstrom, W. M.; Olson, A. J.; Lin, J. H.; Li, W. W.; McCammon, J. A. Remarkable Loop Flexibility in Avian Influenza N1 and Its Implications for Antiviral Drug Design. *J. Am. Chem. Soc.* **2007**, *129*, 7764–7765.
(38) Cheng, L. S.; Amaro, R. E.; Xu, D.; Li, W. W.; Arzberger, P. W.; McCammon, J. A. Ensemble-based virtual screening reveals potential novel antiviral compounds for avian influenza neuraminidase. *J. Med. Chem.* **2008**, *51*, 3878–3894.
(39) Abagyan, R.; Totrov, M.; Kuznetsov, D. ICM—a new method for protein modeling and design: applications to docking and structure prediction from the distorted native conformation. *J. Comput. Chem.* **1994**, *15*, 488–506.
(40) An, J. H.; Lee, D. C. W.; Law, A. H. Y.; Yang, C. L. H.; Poon, L. L. M.; Lau, A. S. Y.; Jones, S. J. M. A Novel Small-Molecule Inhibitor of the Avian Influenza H5N1 Virus Determined through Computational Screening against the Neuraminidase. *J. Med. Chem.* **2009**, *52*, 2667–2672.
(41) Jones, G.; Willett, P.; Glen, R. C.; Leach, A. R.; Taylor, R. Development and validation of a genetic algorithm for flexible docking. *J. Mol. Biol.* **1997**, *267*, 727–748.
(42) Case, D. A.; Darden, T. A.; Cheatham, T. E.; Simmerling, C. L.; Wang, J.; Duke, R. E.; Luo, R.; Crowley, M.; Walker, R. C.; Zhang, W.; Merz, K. M.; Wang, B.; Hayik, S.; Roitberg, A.; Seabra, G.; Kolossváry, I.; Wong, K. F.; Paesani, F.; Vanicek, J.; Wu, X.; Brozell, S. R.; Steinbrecher, T.; Gohlke, H.; Yang, L.; Tan, C.; Mongan, J.; Hornak, V.; Cui, G.; Mathews, D. H.; Seetin, M. G.; Sagui, C.; Babin, V.; Kollman, P. A. *AMBER 10*; University of California: San Francisco, CA, 2008.
(43) Warren, G. L.; Andrews, C. W.; Capelli, A. M.; Clarke, B.; LaLonde, J.; Lambert, M. H.; Lindvall, M.; Nevins, N.; Semus, S. F.; Senger, S.; Tedesco, G.; Wall, I. D.; Woolven, J. M.; Peishoff, C. E.; Head, M. S. A critical assessment of docking programs and scoring functions. *J. Med. Chem.* **2006**, *49*, 5912–5931.
(44) Zaraket, H.; Saito, R.; Sato, I.; Suzuki, Y.; Li, D.; Dapat, C.; Caperig-Dapat, I.; Oguma, T.; Sasaki, A.; Suzuki, H. Molecular evolution of human influenza A viruses in a local area during eight influenza epidemics from 2000 to 2007. *Arch. Virol.* **2009**, *154*, 285–295.
(45) Schmidtke, M.; Riabova, O.; Dahse, H. M.; Stelzner, A.; Makarov, V. Synthesis, cytotoxicity and antiviral activity of *N*,*N*′-bis-5-nitropyrimidyl derivatives of dispirotripiperazine. *Antivir. Res.* **2002**, *55*, 117–127.
(46) Dolinsky, T. J.; Nielsen, J. E.; McCammon, J. A.; Baker, N. A. PDB2PQR: an automated pipeline for the setup of Poisson−Boltzmann electrostatics calculations. *Nucleic Acids Res.* **2004**, *32*, W665–W667.

(47) Dolinsky, T. J.; Czodrowski, P.; Li, H.; Nielsen, J. E.; Jensen, J. H.; Klebe, G.; Baker, N. A. PDB2PQR: expanding and upgrading automated preparation of biomolecular structures for molecular simulations. *Nucleic Acids Res.* **2007**, *35*, W522–W525.
(48) Humphrey, W.; Dalke, A.; Schulten, K. VDM: visual molecular dynamics. *J. Mol. Graphics* **1996**, *14*, 33−38, plates, 27−28.
(49) Shao, J. Y.; Tanner, S. W.; Thompson, N.; Cheatham, T. E. Clustering molecular dynamics trajectories: 1. Characterizing the performance of different clustering algorithms. *J. Chem. Theory Comput.* **2007**, *3*, 2312–2334.
(50) Gasteiger, J.; Rudolph, C.; Sadowski, J. Automatic generation of 3D atomic coordinates for organic molecules. *Tetrahedron Comput. Methodol.* **1990**, *3*, 537–547.
(51) Sadowski, J.; Rudolph, C.; Gasteiger, J. The generation of 3D models of host-guest complexes. *Anal. Chim. Acta* **1992**, *265*, 233–241.
(52) Sadowski, J.; Gasteiger, J.; Klebe, G. Comparison of Automatic Three-Dimensional Model Builders Using 639 X-ray Structures. *J. Chem. Inf. Comput. Sci.* **1994**, *34*, 1000–1008.
(53) DeLano, W. L. *The PyMOL Molecular Graphics System*, version 1.0; DeLano Scientific: Palo Alto, CA, 2002.